Raman Lidar Profiling of Tropospheric Water Vapor over Kangerlussuaq, Greenland

RYAN REYNOLDS NEELY III

Department of Atmospheric and Oceanic Science, University of Colorado, Boulder, Colorado

JEFFREY P. THAYER

Department of Aerospace Engineering Sciences, University of Colorado, Boulder, Colorado

(Manuscript received 3 November 2010, in final form 2 March 2011)

ABSTRACT

A new measurement capability has been implemented in the Arctic Lidar Technology (ARCLITE) system at the Sondrestrom upper-atmosphere research facility near Kangerlussuaq, Greenland (67.0°N, 50.9°W), enabling estimates of atmospheric water vapor through the troposphere. A balloon campaign was simultaneously conducted to calibrate and validate the new lidar water vapor measurements. Initial results show that height-resolved profiles up to 10 km with better than 10% error are obtained with 30-min integration and 250-m height resolution. Comparison of the lidar observations with water vapor profiles retrieved by the Atmospheric Infrared Sounder (AIRS) instrument on board the *Aqua* satellite agree within the error associated with each measurement. These new observations offer more routine measurements of water vapor in the Arctic to complement measurements related to the Arctic's hydrologic cycle.

1. Introduction

Although water vapor is a minor species in the upper troposphere and lower stratosphere, its impact on Earth's atmospheric radiative and chemical budget makes it of major importance. Its distribution influences many physical and chemical properties of the troposphere and stratosphere including polar stratospheric clouds and the Arctic and Antarctic ozone holes. Water vapor is particularly important to Earth's energy budget, influencing both incoming solar radiation and outgoing infrared radiation. Variations in the total amount of atmospheric water vapor are natural and normal but changes in long-term trends in its vertical distribution, especially in the upper troposphere and lower stratosphere, may be indicative of changes in Earth's climate (Houghton et al. 2001). Global trends in stratospheric water vapor concentrations have been identified as a significant contributor to both stratospheric cooling and tropospheric warming (Forster and Shine 2002). Recently upper-tropospheric water vapor has also been recognized as an important driver of decadal global surface climate change and decreases in water vapor over the last decade may have acted to slow the rate of global warming (Solomon et al. 2010).

In addition to its role in the radiation budget, long-term trends in water vapor also play a role in the destruction of ozone through the HO_x cycle. This may also cause changes in the NO_x/ClO_x family, which could further deplete ozone through catalytic reactions during the formation of the Arctic ozone hole (Stenke and Grewe 2005). Also, because of the indirect effect water vapor has on the radiation budget through cloud formation, changes in water vapor can cause changes in heterogenous ozone chemistry through polar stratospheric cloud formation (Stenke and Grewe 2005).

Water vapor profiles of the Arctic atmosphere, where no long-term records exist and current measurements are scarce, are particularly important because climate change has had the largest effect to date in this region (Houghton et al. 2001; Blanchet and Girard 1995; Solomon et al. 2007). More observations are particularly needed to understand the complex set of feedback cycles that involve water vapor as the Arctic atmosphere responds to climate change.

The Arctic Lidar Technology (ARCLITE) facility, a Rayleigh/Mie/Raman lidar system, has been in operation at the Sondrestrom Upper Atmospheric Research

Corresponding author address: Ryan Reynolds Neely III, University of Colorado, ATOC, UCB 311, Boulder, CO 80309-0311.
E-mail: ryan.neely@colorado.edu

DOI: 10.1175/JTECH-D-10-05021.1

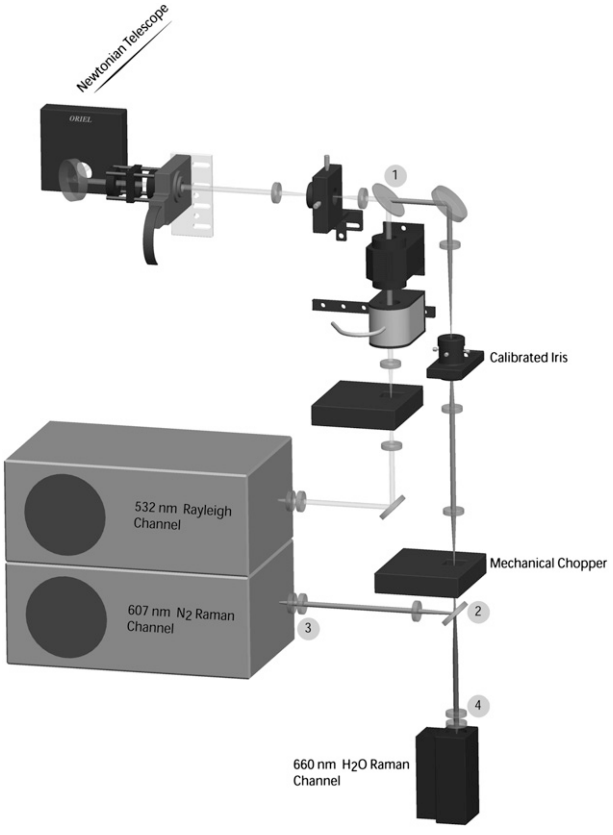

FIG. 1. Depiction of modifications made to the original ARCLITE design, described in Thayer et al. (1997), to enable profiling of water vapor mixing ratio.

Facility, near the town of Kangerlussuaq, Greenland (67.0°N, 50.9°W), since 1993 (Thayer et al. 1997). Molecular and aerosol backscatter is measured at 532 nm to retrieve temperature profiles from 35 to 80 km and aerosol information from the troposphere to the mesosphere. A Raman channel for molecular nitrogen (608 nm) was implemented in 2008 to help determine aerosol extinction values. This allowed the derivation of temperature profiles to be extended into the troposphere. Most recently, a Raman water vapor (661 nm) channel was added in February 2010 to measure water vapor mixing ratio profiles into the upper troposphere and lower stratosphere. Currently, there are few ground-based measurements of water vapor in the upper troposphere and lower stratosphere in the Arctic, but none exist that could be compiled into a climatology. This new capability of the ARCLITE system fills this void in the face of numerous questions about the role of water vapor in climate change. The water vapor analysis of the Raman signals will be the focus of sections 2 and 3, and the derived lidar estimates of water vapor will be calibrated with balloon profiles of water vapor in section 4. In section 5, comparisons will be shown with additional balloon flights and profiles retrieved by the Atmospheric Infrared Sounder (AIRS) satellite.

2. System description

The ARCLITE system employs a monostatic lidar configuration with the transmitter and the center of the telescope separated by about 1.3 m. The ARCLITE transmitter consists of a 30-Hz, 42-W Spectra-Physics Nd:YAG laser, with injection seeding, a second harmonic generator producing 530-mJ pulses at 532.0 nm, and a $\times 5$ beam expander reducing the laser beam divergence to better than 0.1 mrad. The receiver consists of a 92-cm diameter, *f*/2.2 Newtonian telescope, and a side-mounted optical breadboard that holds receiver optics and detectors. The telescope field of view is adjustable but is typically set to 0.5 mrad. This basic layout remains similar to that described by Thayer et al. (1997).

Over time, the ARCLITE system has undergone modifications to enhance its measurement capabilities, including the addition of cross-polarized 532-nm channels for aerosol polarization ratio estimates, and 608- and 661-nm Raman receiver channels. The Raman signals will be the focus of this present work. Figure 1 illustrates a portion of the ARCLITE receiver path that includes the 532-nm Rayleigh/Mie receiver channel and the Raman receiver channel. The salient features for the Raman receiver path are numbered in Fig. 1 and defined in Table 1.

As the 532-nm pulses serve as the excitation wavelength for the Raman-shifted return signals from molecular nitrogen and water vapor, the first dichroic beamsplitter,

TABLE 1. Characteristics of optics used in the two signal channels for the measurement of water vapor mixing ratio. All values are reported as the percent transmission of the particular signal through the optic, unless noted.

Optical component	H_2O (661 nm)	N_2 (608 nm)	Rayleigh–Mie (532 nm)
Rayleigh dichroic splitter	97.5%	97.5%	10^{-3}
Raman dichroic splitter	97.5% (above 655 nm)	80% (reflected below 625 nm)	10^{-6}
Long-pass filters	97.5%	97.5%	10^{-3}
Laser line band stop filters	95%	95%	10^{-6}
608 bandpass filter	10^{-5}	90%	10^{-5}
661 bandpass filter	90%	10^{-5}	10^{-5}

labeled 1 in Fig. 1, reflects the 532-nm signal while transmitting longer wavelengths. A folding mirror directs the longer wavelength signals through a field iris and a mechanical chopper. The mechanical chopper is synchronized with the laser transmitter and blocks near-field signals that may exceed the linearity of the photomultiplier tubes (PMTs). For the Raman signals under study, the near-field signals are geometrically limited by the laser beam/telescope field of view overlap function. The overlap function becomes unity at ranges in excess of 2 km and the Raman signals above those altitudes are weak enough to ensure a linear response by the PMTs. Thus, the chopper is not used in this measurement scheme.

The second dichroic beamsplitter reflects the 608-nm molecular nitrogen Raman signals and passes them through a filter stack that rejects any potential signal contamination by 532-nm signals, as detailed in Table 1. The filter stack consists of a long-pass filter, a 532-nm band-stop filter, and a bandpass filter (0.5 nm centered on 607.7 nm). The 661-nm water vapor Raman signal is transmitted through the dichroic beamsplitter, passes through its filter stack, and is detected by a new Hamamatsu detector, model H7422P-40. The 661-nm filter stack is similar to the 608-nm filter stack except the bandpass filter is 0.5 nm centered at 660.8 nm.

The associated signal transmissions for the three primary wavelengths are detailed in Table 1. A large net rejection (>23 optical density) of the 532-nm (Rayleigh and aerosol) backscattered light ensures little contamination of the Raman signals by the 532-nm signal. This is an important factor when trying to measure the much weaker (10^3 to 10^5 less backscatter) Raman scattered light and derive physical quantities from these measurements on the order of a few parts per million. Without this precaution contamination could easily bias the derived water vapor mixing ratio. The two Raman optical paths are designed to be symmetric so that both channels will have the same near-range overlap function with the telescope. Thus, upon taking the ratio of the two Raman signals, the geometric overlap function, in principle, cancels out. The two PMTs are different and a calibration procedure is discussed in the next section to address this disparity in signal response.

3. Retrieval algorithm

In the Raman water vapor lidar technique (see Whiteman 2003b,a; Sherlock et al. 1999a), the ratio of Raman backscatter from water vapor and molecular nitrogen is proportional to the water vapor mixing ratio. This is possible due to the well-mixed nature of molecular nitrogen in the atmosphere below 80 km. Following the traditional approaches described by Whiteman (2003b,a) and Sherlock et al. (1999a), the water vapor mixing ratio as a function of height, $q(z)$, may be expressed in terms of the two lidar signals (N_x), a calibration constant (C), and a differential transmission term, $\Gamma(z)$:

$$q(z) = C\Gamma(z)\frac{N_{\mathrm{H_2O}} - N_{B,\mathrm{H_2O}}}{N_{\mathrm{N_2}} - N_{B,\mathrm{N_2}}}, \tag{1}$$

where N_x is the total photon counts from each detector and $N_{B,x}$ is the estimated noise counts caused by background skylight and thermal noise of each detector (Sherlock et al. 1999a). Here, $\Gamma(z)$ is an atmospheric differential transmission term, (2), accounting for the wavelength differences in relative extinction of the two Raman backscattered signals. This term is traditionally defined as

$$\Gamma(z) = \frac{\exp\left[-\int_{z0}^{z}\alpha(\lambda_{\mathrm{N_2}}, z')\,dz'\right]}{\exp\left[-\int_{z0}^{z}\alpha(\lambda_{\mathrm{H_2O}}, z')\,dz'\right]}, \tag{2}$$

where α is the wavelength-dependent extinction coefficient (Whiteman 2003b,a; Sherlock et al. 1999a). According to Sherlock et al. (1999a) the error associated with the omission of this term is $\Gamma(z)^{(-1)}$. In the planetary boundary layer, this error is less than 5% and above it drops to less than 0.2%. Because it is such a small factor compared to the relative error from other sources and the fact that reliable simultaneous measurements or models are not available to derive this value, it is assumed to be one for the actual retrieve profiles shown here.

The calibration constant C that accounts for differences in optical path and transmission for the two wavelengths, differing Raman cross sections, and physical constants related to water vapor, air, and molecular nitrogen needed to derive the mixing ratio in (1) and may be defined as

$$C = \frac{\int L_{\mathrm{N_2}}(\lambda)\sigma_{\mathrm{N_2}}(\lambda)}{\int L_{\mathrm{H_2O}}(\lambda)\sigma_{\mathrm{H_2O}}(\lambda)}\frac{M_{\mathrm{H_2O}}}{M_{\mathrm{dryair}}}\frac{n_{\mathrm{N_2}}}{n_{\mathrm{dryair}}}. \tag{3}$$

Here, $L_x(\lambda)$ accounts for differential transmission of the receiving optics (Sherlock et al. 1999a). The differential Raman backscattering coefficient, $\sigma(\lambda)$, of a particular wavelength is in principle a function of temperature and pressure and will vary under different atmospheric conditions. In this retrieval the ratio of the molecular nitrogen to water vapor cross section from Penney and Lapp (1976) is used to derive the calibration constant. Although this parameter is known to vary with atmospheric conditions, principally with temperature (e.g., Whiteman 2003a), this dependence has been omitted. The last two

constants pertain to the conversion or relative numbers of photons to the mixing ratio of water vapor (Whiteman 2003b,a; Sherlock et al. 1999a). The term M_{H_2O}/M_{dryair} is the molecular mass ratio of water vapor to dry air and n_{N_2}/n_{dryair} is the number density fraction of molecular nitrogen in dry air assuming a well-mixed atmosphere (Whiteman 2003b,a; Sherlock et al. 1999a).

An additional correction may be needed to account for the overlap between the telescope and laser for ranges close to the instrument (Halldorsson and Langerholc 1978). The calibration constant C is needed to account for uncertainties in transmissions, reflectivities, and sensitivities of the optical and electronic components. Two balloon-launched Vaisala RS80-H radiosonde profiles have been used to independently derive this single constant. In addition, a separate calibration technique using only the nitrogen signal and physical properties of the measurement was developed. This independent estimate will be shown to have accuracy with an error of similar order to the balloon calibration technique and may be performed routinely to check degradation of the signal paths and detectors over time.

The relative error (4) of the derived mixing ratio profile (1) was found by employing a standard propagation of error techniques to the lidar signal and retrieval algorithm (Thayer et al. 1997):

$$\frac{\sigma_q(z)}{q(z)} = \left[\frac{\sigma_C^2(z)}{C(z)^2} + \frac{\sigma_{R_q}^2(z)}{R_q(z)^2} + \frac{\sigma_\Gamma^2(z)}{\Gamma(z)^2}\right]^{1/2}. \quad (4)$$

The terms contributing to the net relative error are the calibration constant relative error, the lidar signal ratio relative error, and the relative error associated with the uncertainty in the differential transmission; all summed in quadrature assuming the errors are independent and random. The net relative error is predominantly affected by the signal ratio error and the calibration error. The signal ratio error is statistical and assessed assuming Poisson statistics for the lidar signals, where the variance is the mean of the signal counts. Thus, this error relates to the amount of water vapor and molecular nitrogen in the atmosphere and, in general, increases with altitude as a result of decreasing signal levels. The calibration error relates to the method used to determine the calibration constant. This is discussed in more detail in the next section.

4. Calibration

The sensitivity of the Earth's radiation budget to water vapor variations requires accuracy on the order of 3%–10% to fully understand and quantify water vapor–related radiative impacts on climate change (Leblanc and McDermid 2008b). This required accuracy demands signal counts to be large in order to keep the signal ratio percent error in single-digit percentages. This is accomplished by the high-power aperture product of the ARCLITE system and through temporal and range integration. As will be shown, signals integrated for 30 min with a range resolution of 250 m achieve single-digit percent error through the troposphere. The calibration error must also be single-digit percentages to achieve useful water vapor estimates, but has the added complication of possibly introducing systematic errors to the estimate. A common calibration method is to use balloon-launched radiosondes in the local vicinity of the lidar beam to independently estimate water vapor and, thus, retrieve the calibration constant by forcing the lidar estimate to equate to the balloon estimate (Sherlock et al. 1999b; Whiteman et al. 2000). However, balloon instruments have their own inherent set of problems that must be considered when calibrating the system. Therefore, a system calibration procedure was developed to provide a second method for calibration to constrain the systematic effects introduced by the balloon measurement. The second method evaluates lidar system variables that contribute to the calibration constant by performing a signal assessment of the two Raman receiving channels and then deriving the calibration constant. Both methods and their results are described below.

The first attempt at deriving a calibration constant for the new lidar channel was accomplished by using coincident radiosonde, RS80-Hs, measurements and forcing the lidar signal to match the balloon profile within an altitude range containing a relatively high signal-to-noise ratio and homogenous water vapor signal. The accuracy of the humidity measurement on radiosondes has been shown to vary with the sensor type and individual instruments. Especially noteworthy is a dry bias at low humidities and a time lag at low temperatures (Ferrare et al. 1995; Miloshevich et al. 2001). Coincident flights with RS80-H and cryogenic frost point hygrometers at the National Oceanic and Atmospheric Administration (NOAA) Mauna Loa Observatory in Hawaii have shown that the RS80-H deviates where the temperature drops below −55°C (Vömel et al. 2003, 2007). To minimize this effect as well as the dry bias, the radiosondes were flown on relatively wet nights and the upper-tropospheric data were not used for the calibration of the lidar. The altitude range from 3 to 7 km from two balloon flights was used to determine the calibration constant. Between 1 and 3 km the lidar has an incomplete overlap with the telescope so data from this region are not used for calibration. Differences between sonde- and lidar-derived profiles may be due to the spatial and temporal inhomogeneity of water vapor in the atmosphere. This causes physical differences in the

measurement of the sondes and the lidar—the balloons covered a flight path of over 50 km horizontally—which may cause large differences in the concurrent profiles.

An independent calibration is needed to truly determine the accuracy of the lidar measurement (Whiteman et al. 2000; Leblanc and McDermid 2008a). In our second calibration approach, an independent assessment of the two Raman channel detectors and their optical paths was conducted by measuring a redundant nitrogen Raman profile through the optical path of the water vapor channel. This allowed for differences in the optical path, geometric overlap, and PMT gains to be isolated and removed using the relative intensities of the two profiles. When measuring the nitrogen signal along the water vapor path, the final dichroic mirror was removed and the water vapor bandpass filter was replaced by the nitrogen filter (Fig. 1). The error involved in this calibration includes the wavelength differential in the sensitivity of the optics and water vapor PMT to the nitrogen signal. From this information, a calibration constant was derived using only the nitrogen signal. This technique avoids errors associated with the sonde profile calibration technique caused by inhomogeneity of water vapor in the atmosphere because it only depends upon the nitrogen signal, which may be assumed to be well mixed. Although this is not a true absolute calibration of the system, as discussed by Sherlock et al. (1999b) and Whiteman et al. (2000), this method is an alternative to deriving the calibration constant from the traditional radiosonde method. Comparison of the separately derived constants showed less than 5% difference. Given the need for long-term accuracy, as discussed by (Leblanc and McDermid 2008a), and the difficulty of regularly launching radiosondes at this location, the second calibration method discussed above will be implemented on a regular basis to check for system degradation that could cause measurement biases.

5. Validation

Six additional balloon flights occurred during February 2010 after the new water vapor channel was installed and calibrated. These flights followed similar procedures as described by Barnes et al. (2008) and Leblanc and McDermid (2008b). One of the validation flights conducted during February 2010 is shown in Fig. 2. The relative humidity and temperature from the radiosondes have been used to calculate mixing ratio, parts per million by volume (ppmv), using the Vaisala-recommended conversion (Hyland and Wexter 1983). The result of this flight is typical of other intercomparison flights.

The dashed lines in Fig. 2 represent the total error involved in each measurement and, for the majority of the profile, the lidar and radiosonde agree within these bounds. From 2 to 5 km the lidar tracks the layers seen by the radiosonde. This suggests that the feature is a stable layer within the free troposphere. Below 1 km, the deviation of the comparison increases due to the larger variability of water vapor in the planetary boundary layer. A curtain plot of mixing ratio that passed through the lidar beam during the balloon flight is shown in Fig. 3 with an approximate location of the balloon's height with time. The temporal variation we see in this plot may account for the discrepancy seen in comparing the individual balloon profile with the lidar profile in Fig. 2. Given the data, error, and variability, no low-altitude geometric overlap correction was deemed necessary and none has been applied in this analysis.

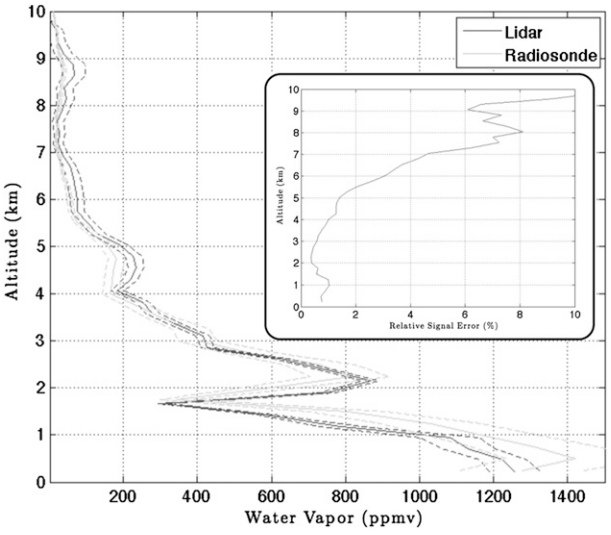

FIG. 2. Water vapor mixing ratio profile comparison between a balloon flight and 30-min integration of lidar signal on 15 Feb 2010. The lidar has been integrated spatially to 250 m to match the balloon data. The subplot is the corresponding signal percent error of the lidar profile. Dashed lines represent the uncertainty associated with each measurement.

An illustration of how the lidar-derived water vapor estimates compare with the six validation balloon flights is given in Fig. 4 in terms of a percent difference. The average percent difference from all six lidar–balloon comparisons is close to zero indicating no apparent bias exists in the calibration constant. Individual balloon–lidar comparisons show deviations (independent with height below 3 km) below 10%. Above 3 km, the lidar tends to become wetter (>2% at 7 km) compared to the balloon measurements. This could be due to a dry bias in the balloons at the colder temperature in the upper polar wintertime troposphere, the omission of a temperature dependence in the backscatter cross sections used to calibrate the lidar, or the small number of samples included in the comparison (Whiteman 2003b; Ferrare

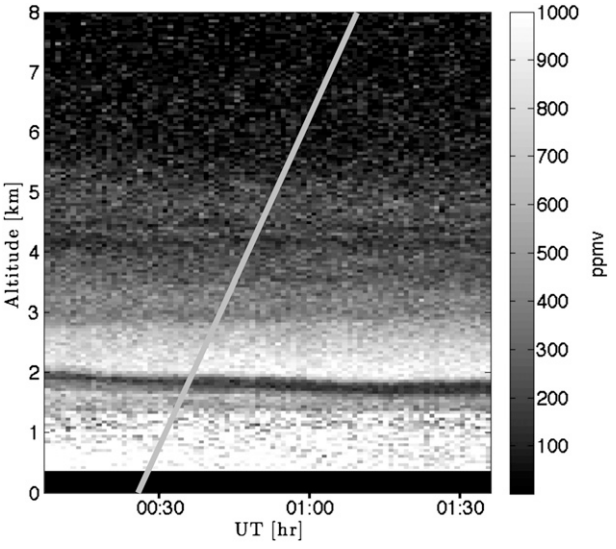

FIG. 3. Curtain plot of water vapor taken on 15 Feb 2010. The line represents the start time and average ascent rate of the balloon flight in Fig. 2.

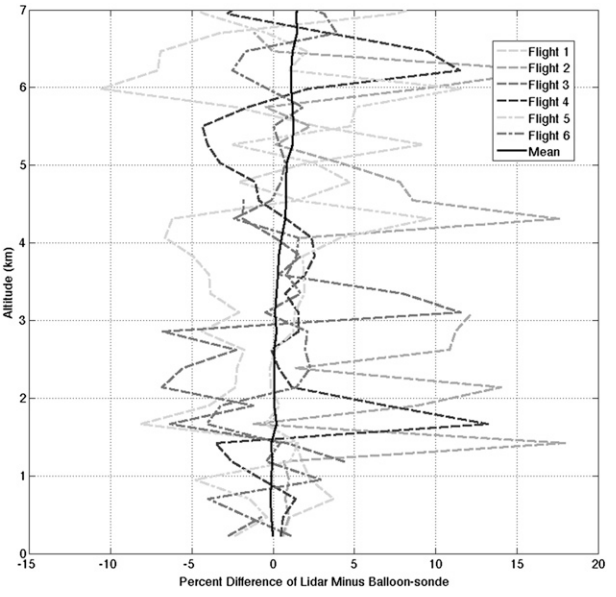

FIG. 4. Percent differences of water vapor profiles derived from the six comparison flights and the lidar profile integrated from 15 min before the launch of the sonde and 15 min after.

et al. 1995; Miloshevich et al. 2001). Furthermore, geophysical variance in water vapor may contribute to the lidar–balloon differences. This comparison leads to the conclusion that the lidar estimate for water vapor concentration is well within 10% uncertainty.

A comparison with version 5 of the atmospheric humidity data collected by the *Aqua* AIRS (Olsen et al. 2007) was conducted as another validation of ARCLITE water vapor profiles. AIRS is a spectrally resolved infrared sounder with 2378 channels covering 650–2675 cm^{-1} that was launched on the Earth Observing System (EOS) *Aqua* satellite on 4 May 2002 and flies in a satellite formation known as the afternoon A train (Read et al. 2007; Olsen et al. 2007). AIRS retrieves H_2O on 28 height levels and, on the basis of radiosonde comparisons, the accuracy of the AIRS humidity data is 15% at 250 mb (Read et al. 2007). Further information and validation of this data product may be found in the work of Read et al. (2007). For the comparison, the AIRS data was screened by the instrument's recommended criteria to ensure the data used were of high fidelity.

A mean AIRS profile is created from profiles taken on 15 February 2010 within 1° of latitude and longitude of the lidar site and within 6 h of the midpoint of the lidar data collection. Comparing AIRS data with the lidar and radiosonde data shows fairly good agreement (Fig. 5). The coarser resolution of AIRS fails to distinguish the detailed structure of the water vapor profile as observed by the radiosonde and lidar, but the AIRS profile does capture the mean trend of the water vapor profile. A comparison with lidar data collected 10 months later (21 December 2010) shows a similar result between the lidar and AIRS data (see Fig. 6). No balloon was launched for this comparison and the calibration used to derive water vapor from ARCLITE was the same as the one derived during the February calibration and validation campaign. This comparison was done to demonstrate the stability of the lidar calibration used in these retrievals.

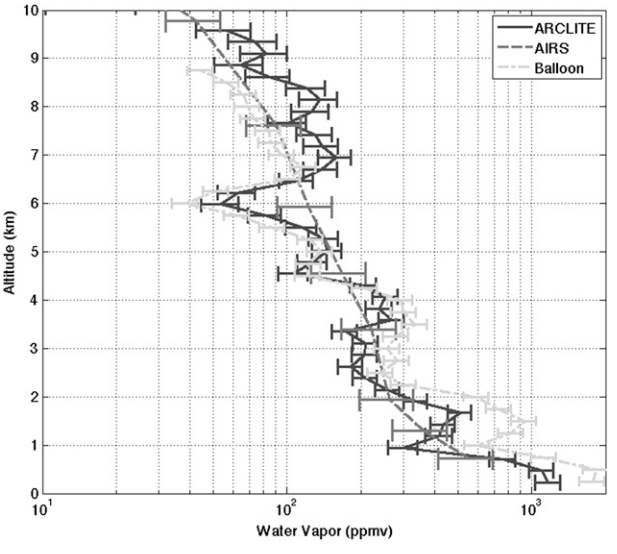

FIG. 5. Comparison of balloon-sonde, ARCLITE, and AIRS during validation campaign on 15 Feb 2010. The AIRS profile is a mean within 1° of the lidar site's latitude and longitude.

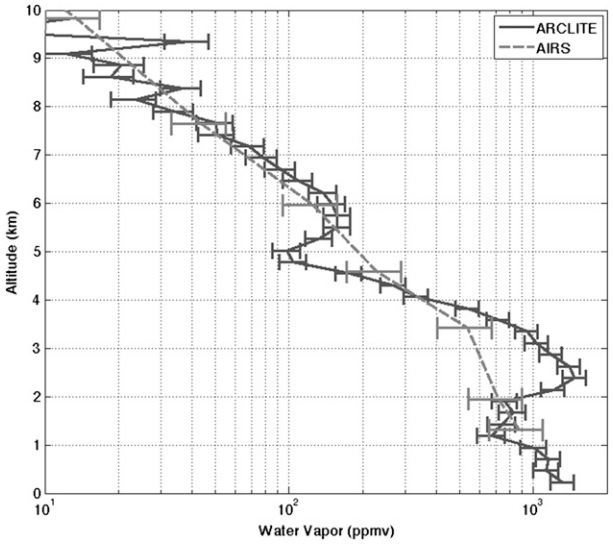

FIG. 6. Comparison of ARCLITE and AIRS on 21 Dec 2010. The AIRS profile is a mean within 1° of the lidar site's latitude and longitude.

6. Conclusions and summary

We have described the design, calibration, and validation of the Raman water vapor profiling channel in the ARCLITE system at the Sondrestrom Upper Atmopshere Research Facility near Kangerlussuaq, Greenland. These initial results suggest the current water vapor profiling setup will provide precise and accurate long-term measurements of water vapor in the upper Arctic troposphere and lower stratosphere. Currently, results show that the lidar is within the range of the 3%–10% levels of accuracy needed to quantify changes in water vapor in order to assess impacts on climate change, as stated by Leblanc and McDermid (2008b). As a result of the dry conditions of the Arctic atmosphere this level of uncertainty is not unexpected and will be validated at a later date with a second balloon comparison campaign, and routine cross measurements of the Raman PMTs will be made to check for detector degradation. The aim of this measurement is to build a climatology of water vapor profiles in order to assess the dynamics of water vapor in the upper Arctic troposphere, a region that has few water vapor measurements but may experience the largest effects. This measurement is of particular importance in light of the recent findings of Solomon et al. (2010) who suggest that stratospheric water vapor is an important driver in global temperature trends.

Acknowledgments. This material is based upon work supported by the National Science Foundation (NSF) under Grant ATM-0454999. Thanks are given to NOAA's Global Monitoring Divisions Ozone and Water Vapor Group (Emrys Hall, Allen Jordan, Dr. Sam Oltsman, Dr. Dale Hurst, and Bryan Johnson) whose help with the balloons made this study possible. We would like to acknowledge Dr. Eric Ray and Dr. Karen Rosenlof for their help in obtaining and understanding the AIRS data. The SRI site crew was also very helpful during this campaign. We would also like to thank Steve Mitchell for his help in documenting the system layout.

REFERENCES

Barnes, J., T. Kaplan, H. Vömel, and W. Read, 2008: NASA/Aura/Microwave Limb Sounder water vapor validation at Mauna Loa Observatory by Raman lidar. *J. Geophys. Res.,* **113,** D15S03, doi:10.1029/2007JD008842.

Blanchet, J., and E. Girard, 1995: Water vapor-temperature feedback in the formation of continental Arctic air: Its implication for climate. *Sci. Total Environ.,* **160,** 793–802.

Ferrare, R., S. Melfi, D. Whiteman, and K. Evans, 1995: A comparison of water vapor measurements made by Raman lidar and radiosondes. *J. Atmos. Oceanic Technol.,* **12,** 1177–1195.

Forster, P. M. de F., and K. P. Shine, 2002: Assessing the climate impact of trends in stratospheric water vapor. *Geophys. Res. Lett.,* **29,** 1086, doi:10.1029/2001GL013909.

Halldorsson, T., and J. Langerholc, 1978: Geometrical form factors for the lidar function. *Appl. Opt.,* **17,** 240–244.

Houghton, J. T., Y. Ding, D. J. Griggs, M. Noguer, P. J. van der Linden, X. Dai, K. Maskell, and C. A. Johnson, Eds., 2001: *Climate Change 2001: The Scientific Basis.* Cambridge University Press, 881 pp.

Hyland, R., and A. Wexter, 1983: Formulations for the thermodynamic properties of the saturated phases of H_2O from 173.15 K to 473.15 K. *ASHRAE Trans.,* **89,** 500–519.

Leblanc, T., and I. McDermid, 2008a: Accuracy of Raman lidar water vapor calibration and its applicability to long-term measurements. *Appl. Opt.,* **47,** 5592–5603.

——, and ——, 2008b: First-year operation of a new water vapor Raman lidar at the JPL Table Mountain Facility, California. *J. Atmos. Oceanic Technol.,* **25,** 1454–1462.

Miloshevich, L., H. Vömel, and A. Paukkunen, 2001: Characterization and correction of relative humidity measurements from Vaisala RS80-A radiosondes at cold temperatures. *J. Atmos. Oceanic Technol.,* **18,** 135–156.

Olsen, E. T., E. Fishbein, S. Granger, S.-Y. Lee, E. Manning, M. Weiler, J. Blaisdell, and J. Susskind, 2007: AIRS/AMSU/HSB version 5 data release user guide. NASA Goddard Space Flight Center, 68 pp. [Available online at http://disc.sci.gsfc.nasa.gov/AIRS/documentation/v5_docs/AIRS_V5_Release_User_Docs/V5_Data_Release_UG.pdf.]

Read, W. G., and Coauthors, 2007: Aura Microwave Limb Sounder upper tropospheric and lower stratospheric H_2O and relative humidity with respect to ice validation. *J. Geophys. Res.,* **112,** D24S35, doi:10.1029/2007JD008752.

Sherlock, V., A. Garnier, A. Hauchecorne, and P. Keckhut, 1999a: Implementation and validation of a Raman lidar measurement of middle and upper tropospheric water vapor. *Appl. Opt.,* **38,** 5838–5850.

——, A. Hauchecorne, and J. Lenoble, 1999b: Methodology for the independent calibration of Raman backscatter water-vapor lidar systems. *Appl. Opt.,* **38,** 5816–5837.

Solomon, S., D. Qin, M. Manning, M. Marquis, K. Averyt, M. M. B. Tignor, H. L. Miller Jr., and Z. Chen, Eds., 2007: *Climate*

Change 2007: The Physical Science Basis. Cambridge University Press, 996 pp.

——, K. H. Rosenlof, R. W. Portmann, J. S. Daniel, S. M. Davis, T. J. Sanford, and G.-K. Plattner, 2010: Contributions of stratospheric water vapor to decadal changes in the rate of global warming. *Science,* **327,** 1219–1223.

Stenke, A., and V. Grewe, 2005: Simulation of stratospheric water vapor trends: Impact on stratospheric ozone chemistry. *Atmos. Chem. Phys.,* **5,** 1257–1272.

Thayer, J., N. Nielsen, R. Warren, C. Heinselman, and J. Sohn, 1997: Rayleigh lidar system for middle atmosphere research in the Arctic. *Opt. Eng.,* **36,** 2045–2061.

Vömel, H., M. Fujiwara, and M. Shiotani, 2003: The behavior of the snow white chilled-mirror hygrometer in extremely dry conditions. *J. Atmos. Oceanic Technol.,* **20,** 1560–1567.

——, D. E. David, and K. Smith, 2007: Accuracy of tropospheric and stratospheric water vapor measurements by the cryogenic frost point hygrometer: Instrumental details and observations. *J. Geophys. Res.,* **112,** D08305, doi:10.1029/2006JD007224.

Whiteman, D., 2003a: Examination of the traditional Raman lidar technique. I. Evaluating the temperature-dependent lidar equations. *Appl. Opt.,* **42,** 2571–2592.

——, 2003b: Examination of the traditional Raman lidar technique. II. Evaluating the ratios for water vapor and aerosols. *Appl. Opt.,* **42,** 2593–2608.

——, T. Berkoff, D. Turner, T. Tooman, R. Ferrare, and L. Heilman, 2000: Research efforts in the absolute calibration of a Raman water vapor lidar. NASA Goddard Space Flight Center, 16 pp. [Available online at http://ramanlidar.gsfc.nasa.gov/activities/publications/data/dnws_Calibration_poster.pdf.]